Q. J. R. Meteorol. Soc. (2004), **130**, pp. 519–539 doi: 10.1256/qj.03.11

Air–sea exchange of sensible heat over the Baltic Sea

By XIAOLI GUO LARSÉN, ANN-SOFI SMEDMAN and ULF HÖGSTRÖM*
Department of Earth Sciences, Uppsala University, Sweden

(Received 16 January 2003; revised 3 July 2003)

SUMMARY

The exchange of sensible heat at the sea surface has been studied with the aid of a comprehensive dataset from the marine site Östergarnsholm in the Baltic Sea, with additional data from another site in the Baltic Sea, Nässkär. The measurements include turbulent fluxes at about 10 m above the water surface, profiles of temperature and wind data at several levels on towers, sea surface temperatures and wave data.

The neutral Stanton number, C_{HN}, was found to follow predictions from surface-renewal theory quite well for unstable conditions up to a wind speed of about 10 m s^{-1}. For higher wind speeds the experimental data deviate to an increasing extent from the prediction based on surface-renewal theory, giving 20–40% higher values at 14 m s^{-1}. The C_{HN} value at 14 m s^{-1} and unstable stratification is about 1.5×10^{-3}; the corresponding value at the same wind speed but with slightly stable conditions is only 0.5×10^{-3}. The interpretation is made that spray is the cause of the rapid increase of heat exchange with wind speed above about 10 m s^{-1}. It also explains the drop in C_{HN} at neutral stability, the spray-mediated sensible-heat flux increasing the upward directed flux of sensible heat in unstable conditions and decreasing the flux in stable conditions.

For stable conditions, C_{HN} data are widely scattered, with a mean of about 0.75×10^{-3}. It appears that the data have an approximate upper bound given by surface-renewal theory. It is suggested that at least some of the strong suppression of the flux of sensible heat during stable conditions can be explained as a shear-sheltering effect caused by the presence of a low-level wind maximum.

KEYWORDS: Marine boundary layer Spray effects Stanton number

1. INTRODUCTION

During the past decades many experiments have been conducted over the ocean in order to determine the fluxes of momentum, heat and moisture at the surface, as these variables are key boundary conditions for coupled atmosphere–ocean models. Although considerable efforts have been spent on the issue, the problem is far from settled; different experiments reported in the literature give seemingly contradictory results. It is common to relate fluxes to more easily measured or calculated mean quantities such as wind speed, temperature and humidity, through the so-called bulk coefficients: the drag coefficient for momentum, C_D, the Stanton number for heat, C_H, and the Dalton number for humidity, C_E. In what follows the three wind components are denoted u, v and w, primed values indicate deviations from the mean, and overbars denote averaging. The bulk coefficients are defined through the following equations:

$$u_*^2 = (\overline{u'w'}^2 + \overline{v'w'}^2)^{1/2} = C_D(U - U_s)^2, \tag{1a}$$

$$\overline{w'\theta'} = C_H(U - U_s)(\theta_s - \theta), \tag{1b}$$

$$\overline{w'q'} = C_E(U - U_s)(q_s - q), \tag{1c}$$

where $\tau = \rho(\overline{u'w'}^2 + \overline{v'w'}^2)^{1/2}$ is the momentum flux (kg m^{-1}s^{-1}), u_* is the friction velocity (m s^{-1}), $\rho C_p\overline{w'\theta'}$ is the sensible-heat flux (W m^{-2}) and $\rho\overline{w'q'}$ is the water vapour flux (kg m^{-2}s^{-1}). U and U_s, are the mean wind speeds (m s^{-1}), θ and θ_s are potential temperatures (K), and q and q_s are mixing ratios ($kg_{H_2O}kg_{air}^{-1}$), each at a reference height, usually 10 m, and at the sea surface, respectively. ρ is air density (kg m^{-3}) and C_p is the specific heat at constant pressure (J kg^{-1}K^{-1}).

* Corresponding author: Uppsala University, Department of Earth Sciences, Air and Water Science, Villavägen 16, S-75273, Uppsala, Sweden. e-mail: ulf.hogstrom@met.uu.se

In this paper focus is on the sensible-heat flux and the corresponding bulk parameter C_H. As in most studies in this field, particular emphasis is placed on C_{HN}, the Stanton number reduced to neutrality (see section 3 for definition). The evidence concerning this parameter is fairly confusing. In unstable conditions, most field experimental studies tend to indicate that C_{HN} is approximately constant, having a value around 1.1×10^{-3}, e.g. Smith (1980), Large and Pond (1982), DeCosmo *et al.* (1996). On the other hand, theoretical approaches, based on so-called surface-renewal theory, combined with laboratory data, e.g. Liu *et al.* (1979), Fairall *et al.* (1996a) and Zeng *et al.* (1998), indicate that C_{HN} should be a slowly decreasing function of wind speed. Recently Andreas and DeCosmo (2002), in a re-analysis of the HEXOS (Humidity Exchange Over the Sea) data of DeCosmo *et al.* (1996), demonstrated that spray is likely to have contributed substantially to the fluxes of sensible heat (and of latent heat) in high-wind conditions, giving the false impression that C_{HN} is independent of wind speed. They assumed that the theoretical expressions based on surface-renewal theory are valid for the turbulent flux at the surface, but with the important addition of a strongly wind-speed-dependent function based on work by Andreas (1992) to take into account the effect of spray. After optimizing the 'nominal' contributions from spray, the authors found that the spray effect starts to be of importance at about 10 m s^{-1}, increasing rapidly in magnitude with wind speed, amounting to about 20–30% of the total flux for cases with wind in the range 15–18 m s^{-1}.

In the present paper, several years' data gathered at the air–sea interaction site at Östergarnsholm in the Baltic Sea are analysed. Turbulent fluxes are measured both with the much used Solent 1012R2 sonic anemometer and with the MIUU (Meteorology Institute Uppsala University) instrument (see below). Also used are data obtained during another marine field experiment in the Baltic Sea at Nässkär. Here the MIUU instrument was exclusively used for turbulence measurements. In section 2 the sites and the data are described; section 3 gives details about the data analysis; section 4 presents the basic results which are further discussed in section 5; whilst section 6 presents the conclusions.

2. Measurement sites and data

(*a*) *The measurement sites*

The main measuring site is the small island of Östergarnsholm, situated 4 km east of the larger island of Gotland in the middle of the Baltic Sea (see Fig. 1). Östergarnsholm is a very low island, with no trees but covered with short grass and herbs. At the southernmost tip of the island a 30 m instrumented tower has been erected. The tower base is about 1 m above mean sea level. The variation of water level in this part of the Baltic Sea is about ±0.5 m, and the heights to the different measuring levels on the tower have been corrected using water-level measurements at Visby harbour, situated on the west coast of the island of Gotland. The distance from the tower to the shoreline is between 5 and 20 m in the southern sector (90°–210°).

The sea floor off the island has a slope of about 1:30 close to the shore, and at about 10 km from the peninsula the water depth is 50 m, exceeding 100 m farther out. In Smedman *et al.* (1999) the possible influence of the limited water depth on the tower measurements was studied in detail. Flux footprint calculations were done, showing that the turbulence instruments 'see' areas far upstream of the island; but still sufficiently long waves 'feel' the presence of the sea floor, implying that peak wave phase speed c_p

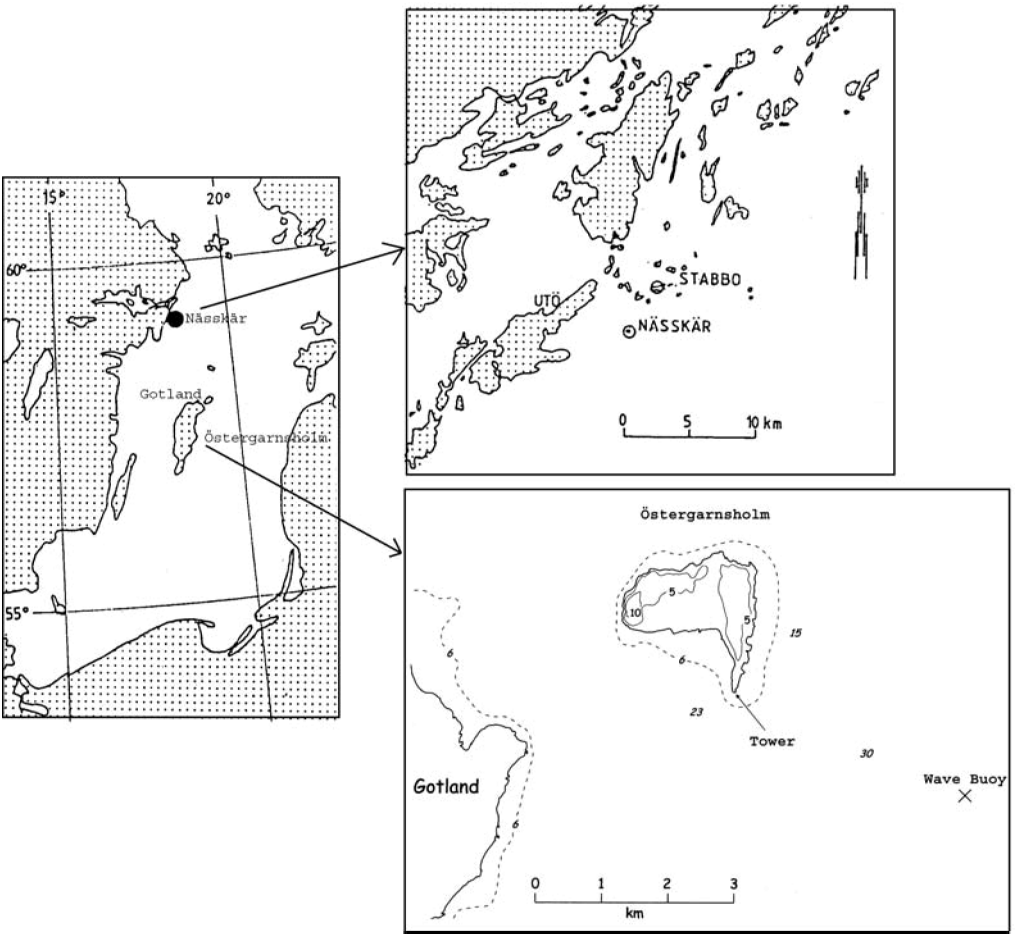

Figure 1. Map showing the locations of the measuring sites Östergarnsholm (57°27′N, 18°59′E) and Nässkär (58°57′N, 18°24′E) in the Baltic Sea, with close-ups of the two sites.

(m s^{-1}) must be calculated using the dispersion relation:

$$c_p = \frac{g}{\omega_o} \tanh\left(\frac{\omega_o h}{c_p}\right), \tag{2}$$

where ω_o is frequency (radian s^{-1}), h is the water depth (m) and g the acceleration due to gravity (m s^{-2}).

Taking the 'footprint weighting function' $F(z)$ from Eq. (A.7) of Smedman *et al.* (1999), it is possible to calculate a weighted mean phase speed

$$\langle c_p \rangle = \int_0^\infty F(x, z,) c_p(x)\, dx. \tag{3}$$

Whenever c_p is used in this paper, it has been calculated using Eq (3).

Smedman *et al.* (1999) found that, although the phase speed of the relatively long waves was indeed influenced by shallow-water effects, little effect on the turbulence structure in the atmospheric surface layer was observed. In Smedman *et al.* (2003) a comparison was made of roughness length z_0 (m) for pure-wind sea conditions

(young waves) from Östergarnsholm and from open-ocean sites. It showed that the Östergarnsholm data agree very well with the corresponding calculations presented in Drennan *et al.* (2002), based on open-ocean data.

A wave rider buoy (owned and run by the Finnish Marine Research Institute) is moored at 36 m depth ~4 km from the tower in the direction 115°, representing the wave conditions in the upwind fetch area (see below).

The other measuring site from which data are taken for the present study is Nässkär, situated in the outer parts of the Stockholm archipelago (see Fig. 1). The island is a flat rock of dimension 20 m × 40 m and maximum height 2 m, with no vegetation. Turbulence measurements with MIUU instruments (see below) were performed on a tower at 8 and 31 m above mean water level; additional, slow-response measurements of wind speed and temperature were made at several levels on the tower. The site has a long (>100 km) open fetch for the sector 60°–220°. Sea surface temperature was measured using a sensor deployed offshore from the island. As this instrument was easily damaged by wave action, the dataset available for studies of bulk heat flux is fairly limited. At this site frequent pilot-balloon measurements were performed, which enabled detailed studies of the effects due to a low-level wind maximum on surface-layer turbulence; see Bergström and Smedman (1995) and Smedman *et al.* (1995) for further details.

(*b*) *Profile instrumentation*

The 30 m tower at Östergarnsholm is instrumented with slow-response profile sensors of in-house design for temperature (Högström 1988) and for wind speed and direction at five heights. The accuracy of the anemometers is 0.2 m s^{-1} and, as shown in Smedman *et al.* (1991), this instrument has negligible over-speeding (i.e. because of careful design of the small and light anemometer cups, the instrument has nearly linear response to velocity changes). Air temperature is measured with 500 ohm platinum-resistance sensors in aspirated radiation shields; measurements are taken of consecutive differences between levels, with an additional sensor at the lowest level for actual temperature. The estimated accuracy of the temperature difference measurements is ±0.02 K (Smedman and Högström 1973; Högström 1988). Humidity is measured at one level (8 m) with a Rotronic sensor. Similar instrumentation was installed at the Nässkär site.

(*c*) *Turbulence instrumentation*

Turbulent fluctuations are measured at three heights at Östergarnsholm with SOLENT 1012R2 (henceforward R2) sonic anemometers (Gill Instruments, Lymington, UK). The R2s were calibrated individually in a big wind-tunnel prior to being installed on the tower. The calibration procedure used is similar to that described by Grelle and Lindroth (1994). After nearly 4 years of operation the R2s were re-calibrated in the same wind-tunnel with almost identical results. From the sonic signals the three orthogonal wind components (u, v, w) and the so called 'sonic temperature' is obtained. As shown in Högström and Smedman (2004), the difference between the flux of sonic temperature and the flux of virtual temperature θ_v, is less than 2% in conditions prevailing at Östergarnsholm. The sonic temperature has been corrected for cross-wind contamination in the way described by Kaimal and Gaynor (1991).

During some periods the MIUU turbulence instrument was also employed at Östergarnsholm. As mentioned earlier, all turbulence measurements at Nässkär were made with this type of instrument. The MIUU instrument is basically a wind-vane-mounted three-component hot-film instrument with additional platinum sensors for

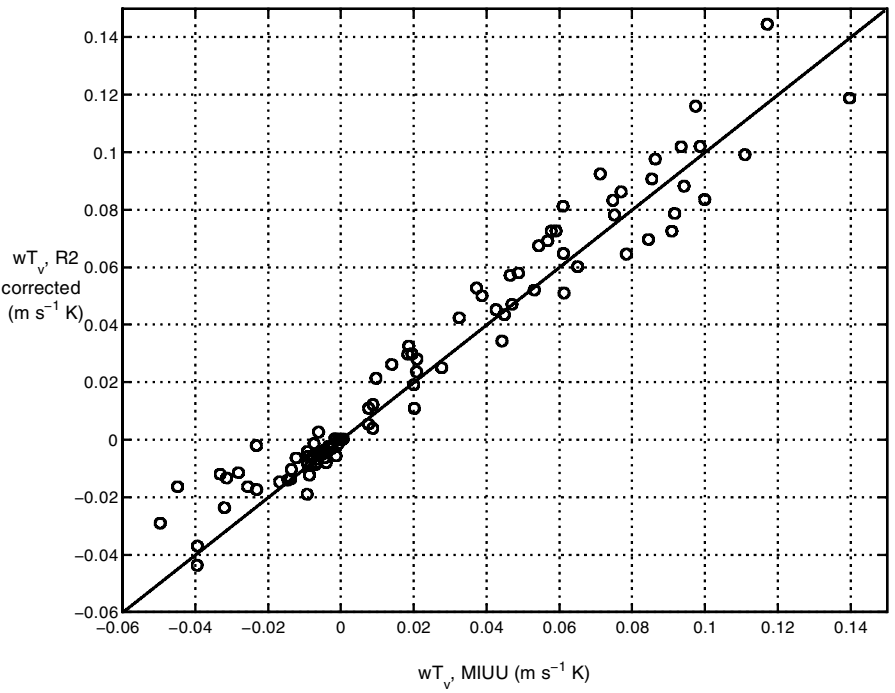

Figure 2. Field intercomparison test of the flux of virtual potential temperature, $\overline{w'T_v'}$, derived from simultaneous measurements with a sonic Solent 1012R2 anemometer (ordinate) and a MIUU instrument (abscissa). See text for details.

dry- and wet-bulb temperatures. The instrument has been carefully investigated for flow distortion (Högström 1988). The corrections employed as a result of this study are very simple, and accurate when compared to corresponding corrections derived for the R2 sonic anemometers. The directional characteristics of the particular hot-film probes used have been investigated in a wind-tunnel study (Bergström and Högström 1987). As demonstrated in Högström (1988) the behaviour of the instrument in the field is very good, in respect of both accuracy and long-term stability, and there is a negligible systematic effect on the fluxes of momentum and sensible heat from sensor separation and other possible sources.

The dry-bulb sensor consists of a long (15×10^{-2} m) platinum wire with a diameter of 15×10^{-6} m, which gives a time-constant of 0.005 s. A high length-to-diameter ratio considerably reduces many of the problems connected with other types of rapid-response and small-resistance sensors (Smedman and Lundin 1986), and the frequency response of up to 5–10 Hz is also sufficient for heat-flux measurements in stable conditions at a height of 10 m. Note, that the salinity in the Baltic Sea is very low, about 6 ppt around Östergarnsholm and even slightly lower than this at Nässkär. This means that we never have problems with salt contamination of the platinum wire as is often reported when such measurements are attempted over the oceans of the world, where salinity is about six times higher. Low salinity is also crucial for successful use of the hot-film technique.

A field intercomparison test of flux measurements by the R2 and the MIUU instruments has been reported in detail by Högström (2001) and Högström and Smedman (2004). Figure 2 shows the result for the sensible-heat flux (or, more precisely, the flux of

virtual potential temperature). The mean ratio of the two estimates is 1.00; the scatter is, however, appreciable. An intercomparison test of three MIUU instruments run side-by-side showed that the sensible-heat flux estimates obtained with this type of instrument has an uncertainty of only 7%. This means that the much larger scatter displayed in Fig. 2 must be due primarily to the uncertainty in the R2 estimate, which is found to be as high as 25%. As shown in Högström (2001) and Högström and Smedman (2004), the field intercomparison tests displayed the same general pattern for all the turbulence characteristics compared: insignificant difference in mean values but much larger scatter in the R2 estimates than in the corresponding estimates obtained with the MIUU instrument. Thus, for the momentum flux the mean ratio is 0.97 but the uncertainty is 35% for the R2 and 8% for the MIUU instrument. As discussed in Högström and Smedman (2004), the field intercomparison results were unexpected in view of much higher precision obtained from the wind-tunnel calibration procedure employed. It was argued that the degradation in measurement precision in the field is very likely due to the sensitivity of the wakes behind the three supporting cylinders of the R2 instrument to the character of the approach flow, the wakes obtained in stationary laminar flow being unrepresentative of the fluctuating natural turbulent flow.

The sampling frequency for turbulence signals is 20 Hz and for profile data 1 Hz; all data are averaged over 60 minutes. For a wind direction sector between 90° and 210° there is an undisturbed over-water fetch of more than 150 km at Östergarnsholm, and data with winds coming from that sector are used exclusively here. A corresponding criterion for the selection of data has been used for Nässkär.

When calculating the flux of sensible heat from the R2 sonic anemometer measurements two corrections must be applied: (i) the temperature signal has to be corrected for cross-wind contamination, and (ii) the sonic temperature or, almost equivalently, the virtual temperature, has to be converted to 'ordinary temperature'. The correction has been applied directly to the virtual heat flux using the following formula (Lumley and Panofsky 1964):

$$\overline{w'\theta'} = \frac{\overline{w'\theta'_{\mathrm{v}}}}{1 + 0.07/\beta}, \tag{4}$$

where β is the Bowen ratio $= H/E\lambda \approx C_{\mathrm{p}}\Delta\theta/\lambda\Delta q$, where H is the sensible-heat flux and $E\lambda$ the flux of latent heat (W m^{-2}); $\Delta\theta = \theta_{\mathrm{s}} - \theta(z)$, and $\Delta q = q_{\mathrm{s}} - q(z)$, where q_{s} is the mixing ratio ($\mathrm{kg_{H_2O}kg_{air}^{-1}}$) at the temperature of the surface, T_{s} (K). For the present dataset, the average correction from Eq. (4) is about 11%.

As the MIUU turbulence instrument measures temperature with a platinum wire, no corrections are needed for temperature or heat flux, but when calculating the Obukhov length, L (Eq. (7) below), the heat flux must be converted to virtual heat flux.

(*d*) *Wave data*

Wave data are recorded every hour, and a 1600 s time series is used to calculate a directional spectrum. The spectrum contains 64 frequency bands ranging from 0.05 to 0.58 Hz, with the peak frequency determined by a parabolic fit.

The bucket sea surface temperature, T_{w}, is measured from the wave buoy at a depth of 0.5 m. Fairall *et al.* (1996a,b) gave an algorithm for correcting T_{w} to sea surface temperature, T_{s}, for the TOGA-CORE† experiment in a tropical region. Rutgersson *et al.* (2001) applied the same algorithm to the Östergarnsholm data and found a maximum correction of only 0.15 K.

† Tropical Ocean–Global Atmosphere Coupled-Ocean Atmospheric Response Experiment.

A frequently used parameter to describe the wave state is the so-called wave age parameter c_p/u_* or c_p/U_c where $U_c = U_{10}\cos\varphi$, with φ the direction difference between the wind and the dominating wave, and c_p the phase velocity of the dominant wave at the peak frequency in the wave spectrum.

(*e*) *Data selection*

The Östergarnsholm station has been running semi-continuously since May 1995, but there have been several long breaks in the recordings, especially in the wave measurements during wintertime because the buoy was removed during periods with a risk of ice damage. Data from the years 1995–99 have been used for R2 measurements. The MIUU instrument was in operation during three short periods, in June 1995, October 1998 and November 1999. Data from Nässkär are from two periods in 1981 and 1982. All data (both sites) must satisfy the following criteria.

(i) Datasets of meteorological and wave measurements are complete.

(ii) Wind is from the undisturbed sector (Östergarnsholm: 90°–210°; Nässkär: 60°–220°).

(iii) Wind speeds at all levels are greater than 1.5 m s^{-1}.

(iv) The magnitude of the temperature difference between the 10 m level and the sea surface, $\Delta T = |\theta_{10} - T_w|$ is larger than 1.5 K for cases with R2 measurements, and 1.0 K for most cases with MIUU instrument (for certain occasions with MIUU instrument and stable stratification (May–June 1995) ΔT_{min} has been set to 0.5 K).

(v) For the magnitude of the temperature flux, $H_T = |\overline{w'\theta'}|$, the following criteria have been used: for the R2 measurements, $H_{T\,min} = 0.01$ K m s^{-1} for unstable and 0.005 K m s^{-1} for stable conditions; for the measurements with the MIUU instrument, $H_{T\,min} = 0.001$ K m s^{-1} for both stable and unstable conditions.

3. Theory

(*a*) *Monin–Obukhov similarity theory*

Equation (1b) defines the Stanton number C_H. Traditionally it is assumed that Monin–Obukhov similarity theory (MO) can be applied to the air layer between the water surface and a reference level z, usually set to 10 m. We start out with the simple case when this is strictly true and in later subsections discuss possible additional mechanisms that could alter the situation.

According to MO, the vertical variation of normalized wind speed and temperature can be expressed as unique functions of the stability parameter z/L:

$$\frac{\kappa z}{u_*}\cdot\frac{\partial U}{\partial z} = \phi_m(z/L), \qquad \frac{\kappa z}{T_*}\cdot\frac{\partial \theta}{\partial z} = \phi_h(z/L), \tag{5}$$

where T_* $(= -\overline{w'\theta'}/u_*)$ is the temperature-scale (K), and L is the Obukhov length-scale:

$$L = -\frac{u_*^3 T_0}{\kappa g \overline{w'\theta'_v}}. \tag{6}$$

Here T_0 is the mean temperature of the surface layer (K), κ is von Karman's constant $(= 0.40)$, and $g = 9.81$ m s^{-2}. Integration of Eq. (5) gives mean variables at height z:

$$U(z) - U_s = (u_*/\kappa)\{\ln(z/z_0) - \psi_m\}, \tag{7}$$

$$\theta(z) - \theta_s = (T_*/\kappa)\{\ln(z/z_{0T}) - \psi_h\}, \tag{8}$$

where z_0 and z_{0T} are the roughness lengths for momentum and heat, at which heights the extrapolated wind speed and temperature approach their surface values U_s and θ_s. U_s is generally not larger than 10^{-2} m s^{-1} and is usually set to zero; ψ_m and ψ_h are the integrated analytical forms of the non-dimensional gradients, ϕ_m and ϕ_h respectively:

$$\psi_m(z) = \int_0^{z/L} \{1 - \phi_m(\varsigma)\}/\varsigma \cdot d\varsigma, \tag{9a}$$

$$\psi_h(z) = \int_0^{z/L} \{1 - \phi_h(\varsigma)\}/\varsigma \cdot d\varsigma, \tag{9b}$$

where $\varsigma = z/L$.

From Eqs. (1a), (1b), (7) and (8), the bulk exchange coefficients can be written as:

$$C_D = \frac{\kappa^2}{\{\ln(z/z_0) - \psi_m\}^2}, \tag{10}$$

$$C_H = \frac{\kappa^2}{\{\ln(z/z_0) - \psi_m\}\{\ln(z/z_{0T}) - \psi_h\}}, \tag{11}$$

concerning the ϕ_m and ϕ_h functions, see subsection 3(b).

According to Eqs. (10) and (11), the transfer coefficients for momentum and heat for neutral stratification are:

$$C_N = \frac{\kappa^2}{\{\ln(z/z_0)\}^2}, \tag{12}$$

and

$$C_{HN} = \frac{\kappa^2}{\{\ln(z/z_0)\}\{\ln(z/z_{0T})\}}. \tag{13}$$

(*b*) *The effects of waves on the exchange process*

In a series of papers from the Östergarnsholm project, e.g. Smedman *et al.* (1999), Rutgersson *et al.* (2001) and Smedman *et al.* (2003), it has been demonstrated that the surface waves influence the exchange processes in the marine atmospheric boundary layer (the MABL) to a great extent. As shown in these papers, the wave influence appears to be strongly dependent on wave age. Thus, for growing-sea conditions, when $c_p/U_{10} < 0.8$, there is generally little difference between the exchange process in the MABL and in a corresponding boundary layer over land, but when longer waves become dominant, i.e. for $c_p/U_{10} > 0.8$, the exchange process is being gradually modified for increasing values of c_p/U_{10}. As demonstrated below, this is primarily observed for the momentum exchange during unstable conditions. In the analysis presented in section 4, explicit formulations of ϕ_m and ϕ_h enter the equations for calculation of the roughness length for momentum, Eq. (7), and for heat, Eq. (8).

In Fig. 3, ϕ_m curves are given as a function of z/L for measurements during three wave state conditions representing, respectively: group (I) growing sea (filled circles), group (II) mature sea (pluses), and group (III) swell (open circles). As can be seen from Fig. 3, curve (I) is relatively close (cf. below) to the overland reference curve (solid line) while, with increasing amount of long waves, the ϕ_m values decrease (curves (II) and (III)). Empirical curves of ϕ_m as functions of z/L have been fitted to the data for each of the curves (II) and (III):

$$\phi_m = 1 - (-\beta z/L)^{1/2} \quad \text{for } (z/L)_c < z/L < 0, \tag{14}$$

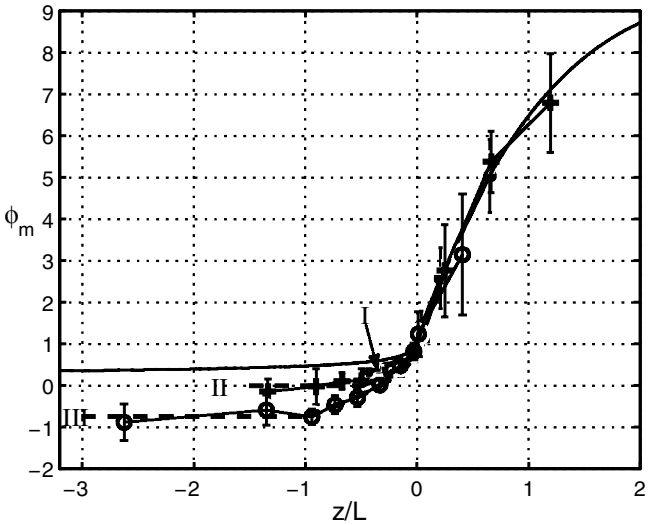

Figure 3. Non-dimensional wind gradient, ϕ_m, from Östergarnsholm at 10 m, plotted as a function of stability parameter z/L. The three symbols represent different wave state conditions: (•) growing sea, (+) mature sea, and (◯) swell. Curves have been drawn to connect the measurement points. Also drawn are two curves that represent typical conditions found over land (Högström 1996). See text for further details.

where β is a parameter that varies with wave state and $(z/L)_c$ is the value where the curves more or less level off (see below). Approximately: $\beta = 2$ for a mature sea (curve (II)) and $\beta = 3$ for swell conditions (curve (III)). For groups (II) and (III), when $z/L < (z/L)_c$, ϕ_m can be described approximately by a constant $C_{ii} = 0$ for $z/L < (z/L)_c = -0.5$, and $C_{iii} = -0.73$ for $z/L < (z/L)_c = -1$. Assuming that Eq. (14) is valid in the entire layer from 10 m down to the water surface, integration of Eq. (14) gives:

$$\psi_m = 2(-\beta z/L)^{1/2} \quad \text{for } (z/L)_c < z/L < 0, \tag{15}$$

with $\beta = 2$ and 3 for groups (II) and (III) respectively. For group (II) and $z/L < (z/L)_c = -0.5$:

$$\psi_m = \ln(|z/L|) - \ln(0.5) + 2. \tag{16a}$$

For group (III) and $z/L < (z/L)_c = -1$:

$$\psi_m = 1.73 \cdot \ln(|z/L|) + 3.464. \tag{16b}$$

The data for group (I), unstable conditions, are between the land curve and the curve representing group (II). Other information from the measurements at Östergarnsholm (Smedman *et al.* 2003) suggests, however, that the influence from waves on a growing sea on the exchange process is very little if any. Therefore we chose to employ the ϕ_m function suggested by Högström (1996):

$$\phi_m = (1 - 19z/L)^{-1/4}, \quad z/L < 0. \tag{17}$$

As discussed in subsection 3(c), the observed slight suppression of the data for group (I) in Fig. 3 may be caused by another effect.

In stable air, the effect of sea state on the turbulence structure is negligible and the expression of Högström (1996) is used:

$$\phi_m = 1 + 5.3z/L, \quad 0.5 \geqslant z/L > 0. \tag{18}$$

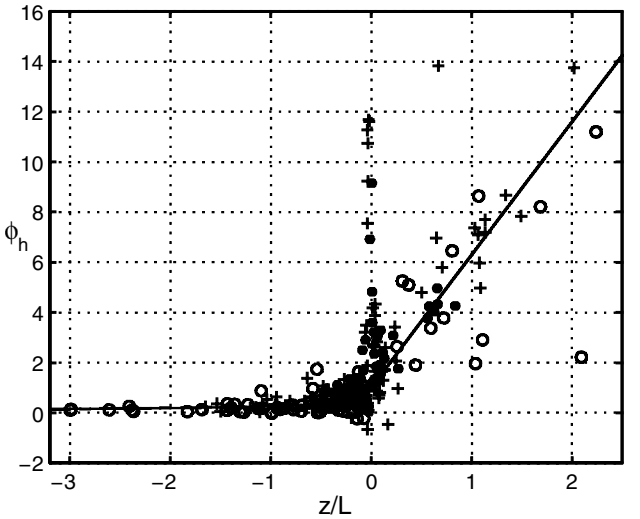

Figure 4. Non-dimensional potential-temperature gradient ϕ_h, from Östergarnsholm at 10 m, plotted as a function of stability parameter z/L. Three symbols represent different wave state conditions: (•) growing sea, (+) mature sea, and (◯) swell. The curves drawn are those recommended by Högström (1996). See text for further details.

Figure 4 shows ϕ_h at 10 m for Östergarnsholm plotted as a function of z/L. Three symbols indicate different wave states. Around neutral, there are some very high values, which arise from dividing small potential-temperature gradients by small heat flux. (Note, that this particular plot was based on a dataset with slightly different criteria than the rest of the study, with particular emphasis on complete temperature profile data; no lower limit for the magnitude of the heat flux was employed.) Apart from that, data gather reasonably well around the curves drawn for unstable and stable conditions, which are based on the equations recommended by Högström (1996). Little, if any, subdivision according to wave state can be observed in the graph. Johansson (2003) has also analysed ϕ_h at 16 and 24 m at Östergarnsholm, and finds that the similarity observed at 10 m (Fig. 3) does not apply to the higher levels. For determination of ψ_h at 10 m, Eq. (9b), knowledge of the variation of ϕ_h in the layer below 10 m is needed. In order to do that integration, we make the assumption that the equations found to be valid at 10 m are also valid down to the surface.

(*c*) *Effects of the depth of the convective boundary layer*

A combination of large-eddy simulations and analysis of field data at a land site, presented in Johansson *et al.* (2001), shows that ϕ_m in the surface layer during unstable conditions is a function not only of z/L, as stated in Eq. (5), but also of z_i/L, where z_i is the height of the convective boundary layer. Thus, a plot of ϕ_m against z/L (Fig. 7 of Johansson *et al.* 2001) shows stratification of the data in bands according to z_i/L. An exactly analogous result was later obtained by Johansson (2003) for measurements at Östergarnsholm. A similar but less pronounced dependence on z_i/L was also found for ϕ_h in these two studies.

Unfortunately, information on the depth of the convective boundary layer is not available at Östergarnsholm and Nässkär on a regular basis. For that reason, we do not attempt a parametrization of this effect in the present study. It is, however, important to

keep in mind that it is likely to contribute considerably to the scatter of every plot where calculation of ϕ_m is involved, notably Eq. (7) which will be used for determination of the roughness length z_0. This uncertainty is also the reason why we disregard the relatively small offset of the curve for a growing sea from the land curve, Eq. (17).

(*d*) *The effect of spray*

The effect of spray on the exchange of sensible and latent heat has been the subject of intensive discussion in the literature over the last few decades, without any consensus being reached, see Andreas (1992) for a comprehensive review. The results of the experimentally very careful HEXOS investigation (DeCosmo *et al.* 1996) were interpreted by the authors as giving no evidence for spray effects for $U_{10} < 20$ m s^{-1}. As mentioned in the Introduction, Andreas and DeCosmo (2002) have, however, re-analysed the HEXOS data and come to the conclusion that there is indeed an effect of spray for $U_{10} > 10$ m s^{-1}. Their analysis is based on a combination of two basic ideas: (i) The neutral Stanton number, C_{HN}, for the exchange of sensible heat in the *absence* of spray is well described by the COARE algorithm by Fairall *et al.* (1996a) for all wind speeds (at least up to 20 m s^{-1}); (ii) *The effect of spray* can be obtained from a modified version of the model of Andreas (1992). The COARE model gives a maximum for C_{HN} at around 8 m s^{-1} (see Fig. 4 of Andreas and DeCosmo 2002). But the HEXOS C_{HN} is constant for $U_{10} < 20$ m s^{-1}. A good overall fit of the HEXOS data for all wind speeds is obtained by optimizing three constants in the model of Andreas (1992), see below.

The spray model of Andreas (1992) and Andreas and DeCosmo (2002) is based on complicated microphysical calculations. Basically, three time-scales are defined, which characterize the evolution of spray droplets as a function of drop diameter and wave height. The most crucial parameter is, however, the spray-generation function. Expressions for this for several drop diameter intervals are given in Andreas (1992). The calculations give spray contributions to the flux of latent heat, $\overline{Q}_L$ and sensible heat $\overline{Q}_S$. In Andreas and DeCosmo (2002) it is hypothesized that 'the total turbulent fluxes at the top of the Droplet Evaporation Layer' can be partitioned as:

$$H_{L,T} = H_L + \alpha \overline{Q}_L, \tag{19a}$$

$$H_{S,T} = H_S + \beta \overline{Q}_S - (\alpha - \gamma)\overline{Q}_L, \tag{19b}$$

where H_S and H_L come from bulk aerodynamic estimates. The parameters α, β, γ were determined by optimization of the HEXOS data to be 4.3, 6.5 and 3.8, respectively. For further details the reader is referred to the original papers.

Unfortunately, the spray model of Andreas (1992) cannot be simply reconstructed from the published papers. In section 4 a general discussion of possible spray effects in our data will be made on the basis of plots of C_{HN} against wind speed.

(*e*) *The effect of shear sheltering*

In Smedman *et al.* (1995) it was observed that the turbulence structure in the stable marine surface layer was significantly affected by the presence of a low-level wind maximum. In Smedman *et al.* (2004) it was argued that the physical mechanism causing the observed reduction in turbulence and turbulent transport is shear sheltering, Hunt and Durbin (1999). As described in detail in that paper and in Smedman *et al.* (2004), the fundamental mechanism is that a strong shear layer has the characteristics of a vortex sheet which, provided certain criteria are fulfilled, will exert an upward directed force on an eddy moving towards it, thus preventing the eddy from penetrating further

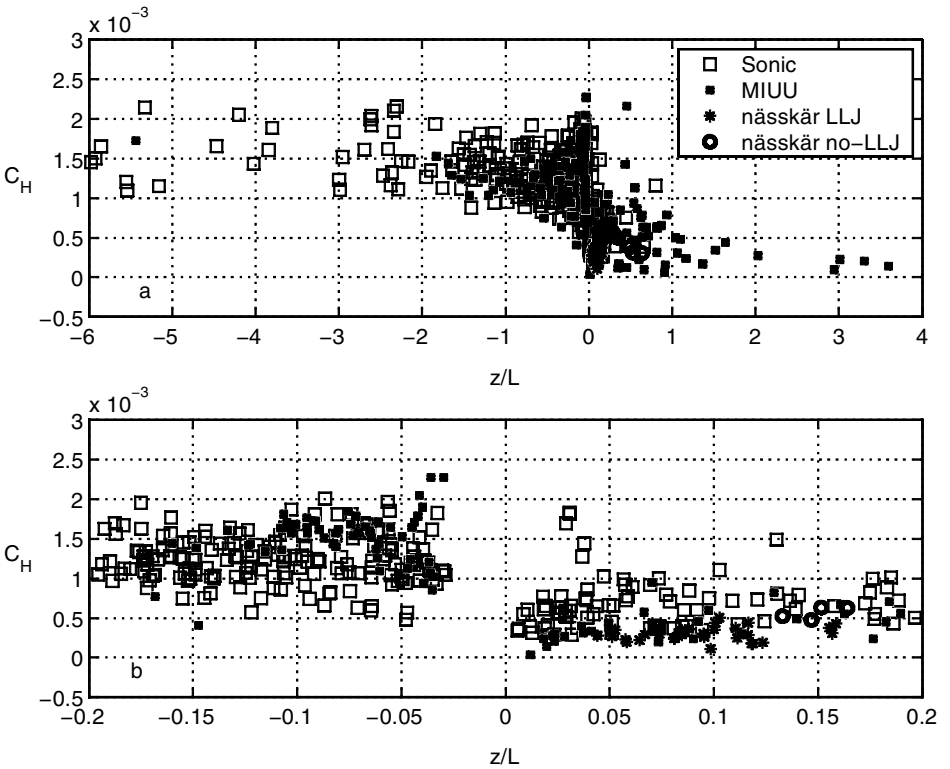

Figure 5. The Stanton number C_H, plotted against stability parameter, z/L: (a) for the entire stability range, (b) for $-0.2 < z/L < 0.2$. 'Sonic' refers to data obtained with the Solent 1012R2 sonic anemometer; 'MIUU' indicates data obtained with the MIUU instrument at Östergarnsholm; 'Nässkär LLJ' means cases with, and 'Nässkär no-LLJ' cases without, a low-level jet maximum observed somewhere in the layer 40–300 m. All data from Nässkär were obtained with the MIUU instrument. See text for further details.

downwards. The result will be suppression of low-frequency energy below the shear layer. As relatively large eddies are known to be responsible for much of the turbulent exchange, it is reasonable to expect that this mechanism may result in a reduction of the turbulent flux near the surface. In section 4 some data for cases with stable stratification can be stratified according to the presence or absence of a low-level wind maximum, so this possible effect of shear sheltering on the exchange of sensible heat can be checked.

4. Results

In this section the results of the data analysis are presented by means of a number of figures. Remarks are made about prominent features, but interpretation of the results is postponed until section 5.

Figure 5(a) shows C_H plotted as a function of z/L for the entire stability range, and Fig. 5(b) similarly for the near-neutral range, $-0.2 < z/L < 0.2$. Here C_H has been derived from the defining Eq. (1b) from measured temperature fluxes $\overline{w'\theta'}$, simultaneous temperature differences $\theta_s - \theta_{10}$, and wind speed U_{10}, assuming the mean wind speed at the water surface, U_s, to be zero. Two features are particularly striking in Fig. 5: (i) a significant change of the mean level for C_H at $z/L = 0$; and (ii) the more uncertain data obtained from the R2 sonic anemometer measurements (the squares) tend to scatter mainly below the MIUU data on the unstable side and above the MIUU data on the

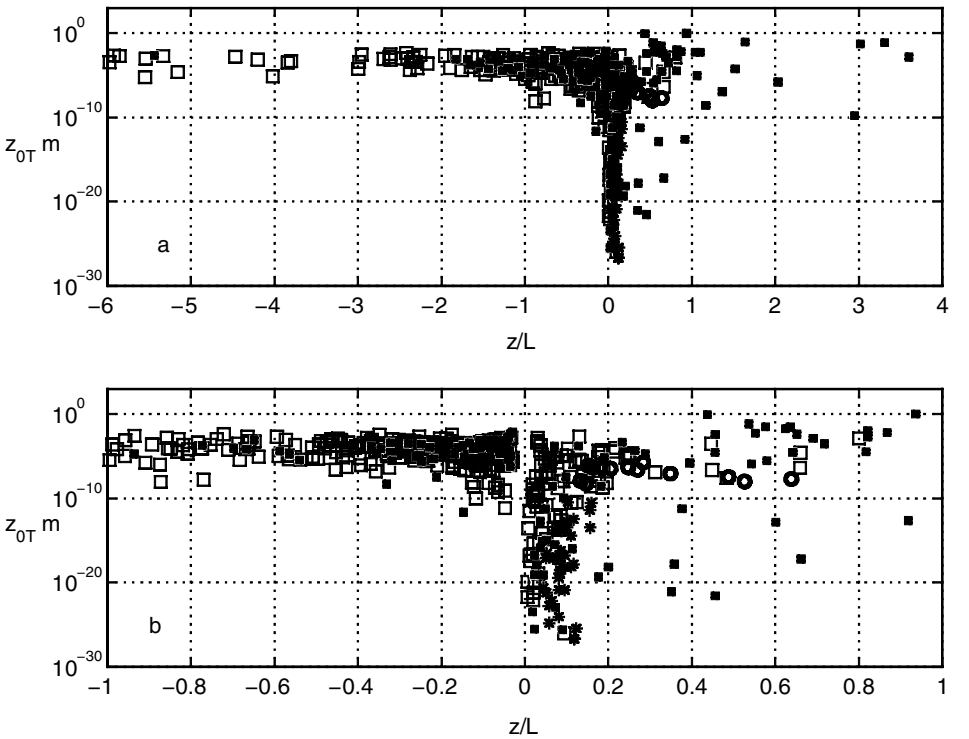

Figure 6. Roughness length for heat, z_{0T}, plotted as a function of stability parameter, z/L (see section 3), for two stability ranges: (a) $-6 < z/L < 4$, and (b) $-1 < z/L < 1$. Symbols are as in Fig. 5.

stable side of Fig. 5(b). Considering the transition of the more reliable MIUU data in the near-neutral range, a more distinctive pattern is observed compared to the overall pattern, dominated by the more uncertain R2 data.

In order to enable conversion of C_{H} into C_{HN} through Eq. (13), the roughness length for momentum, z_0, and for sensible heat, z_{0T}, must be determined. Thus z_0 is obtained using Eq. (7) from: measurements of U_{10}; friction velocity u_* obtained from the turbulence measurements with the middle member of Eq. (1a); and the integrated stability function ψ_{m}, Eq. (9a), derived using the $\phi_{\mathrm{m}}(z/L)$ functions specified in subsection 3(b). In a corresponding way, z_{0T} is derived with Eq. (8) from: measurements of the mean temperature difference $\theta_{\mathrm{s}} - \theta_{10}$; eddy correlation measurements of heat and momentum flux to give $T_* = -\overline{w'\theta'}/u_*$; and the integrated stability function ψ_{h}, Eq. (9b), see subsection 3(b). In Smedman *et al.* (2003) it was shown that, for neutral conditions, a logarithmic profile was found at Östergarnsholm only during growing-sea conditions. Nevertheless, in that paper an *apparent* z_0 value was derived from measured values of U_{10} and u_* from the log law for all neutral cases. In this paper a corresponding *apparent* z_0 value is obtained from Eq. (7), which strictly assumes MO theory to be valid in the layer 0 to 10 m above the water surface. In the following, the z_0 and z_{0T} values are all 'apparent' in this sense, and it is not mentioned again.

Figures 6(a) and (b) show the roughness length for heat, z_{0T}, plotted as a function of z/L for the stability ranges $-6 < z/L < 4$, and $-1 < z/L < 1$, respectively. It is found that z_{0T} is constant and about 10^{-5} m for almost the entire unstable range. For slightly stable conditions there is a dramatic drop in z_{0T} amounting to many orders

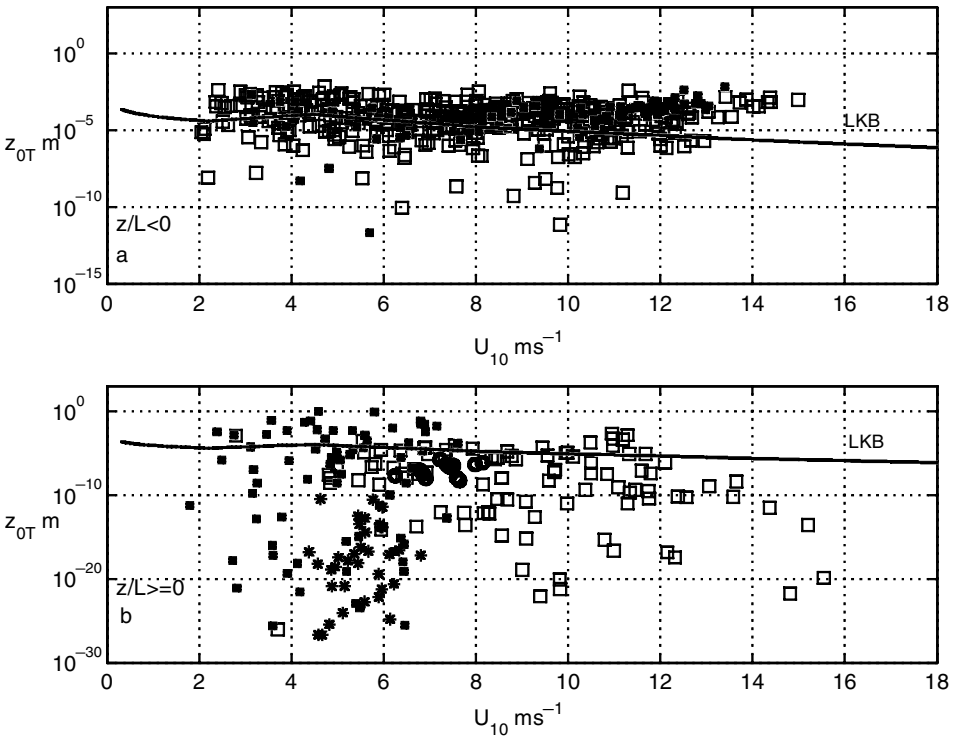

Figure 7. Roughness length for heat, z_{0T}, plotted as a function of wind speed at 10 m for: (a) stability parameter, $z/L < 0$, and (b) $z/L > 0$ (see section 3). The curve denoted LKB is from Liu *et al.* (1979). Symbols are as in Fig. 5.

of magnitude. For $z/L > 0.2$, z_{0T} appears to go back to values similar to that typical of unstable conditions, although the scatter is appreciable. In Fig. 7, z_{0T} has been plotted against wind speed at 10 m; Figs. 7(a) and (b) represent unstable and stable conditions, respectively. No clear variation with wind speed can be found in the graphs. For unstable conditions, the vast majority of the data cluster within a narrow range of z_{0T} values, with occasional low values occurring at all wind speeds. The line drawn in Fig. 7(a) is based on the prediction by Liu *et al.* (1979) from surface-renewal theory. The data are in agreement with this prediction for $U_{10} < 8$ m s^{-1} but deviate systematically with increasing wind speed. This feature will be discussed later.

Figure 8 shows the aerodynamic roughness length, z_0, plotted as a function of stability; Figs. 8(a) and (b) give data for the entire stability range and for the range $-0.2 < z/L < 0.2$, respectively. The most prominent feature in this representation is a flat maximum around neutral stability with high values extending well into stable conditions, thus showing a very different pattern than the corresponding plots for z_{0T} in Fig. 7. The natural logarithm of the ratio between z_0 and z_{0T} is shown as a function of z/L in Fig. 9. It shows that the ratio z_0/z_{0T} is of the order 10^{-5} for strong instability (although with large scatter), increasing gradually to values near unity at small $-z/L$. For small positive z/L the ratio becomes extremely large, getting back to ratios near unity for $z/L = 0.2$, albeit with very large scatter.

Knowing z_0 and z_{0T}, it is possible to determine C_{HN} from Eq. (13). Figures 10(a) and (b) show C_{HN} plotted as a function of z/L for the entire stability range $-6 < z/L$

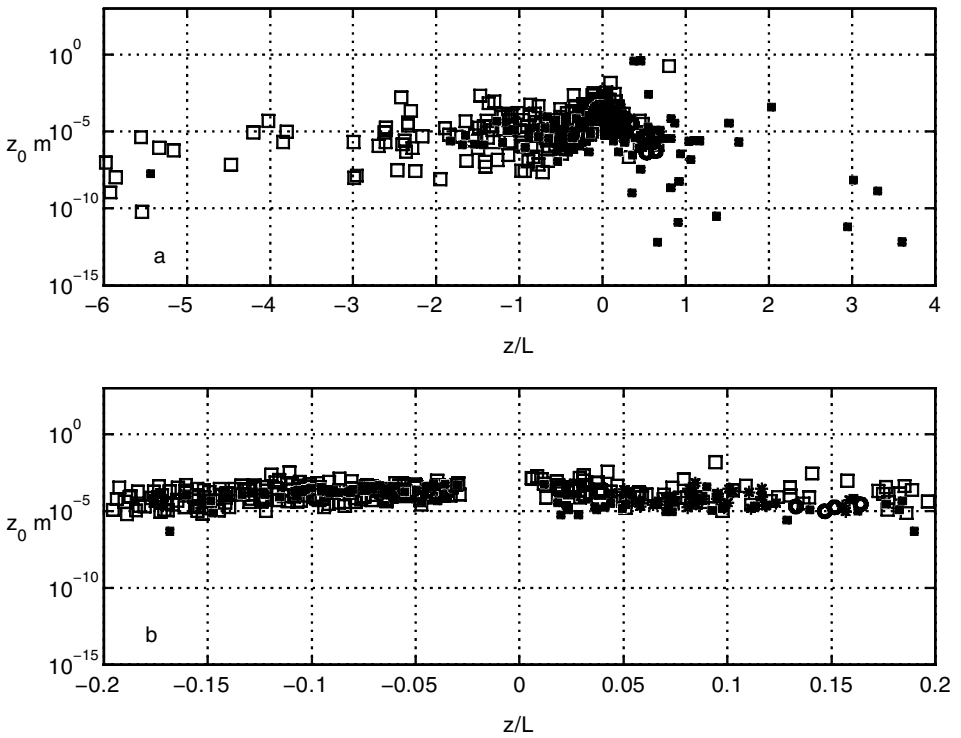

Figure 8. The roughness length for momentum, z_0, plotted as a function of stability parameter, z/L (see section 3), for: (a) the entire stability range, (b) $0.2 < z/L < 0.2$. Symbols are as in Fig. 5.

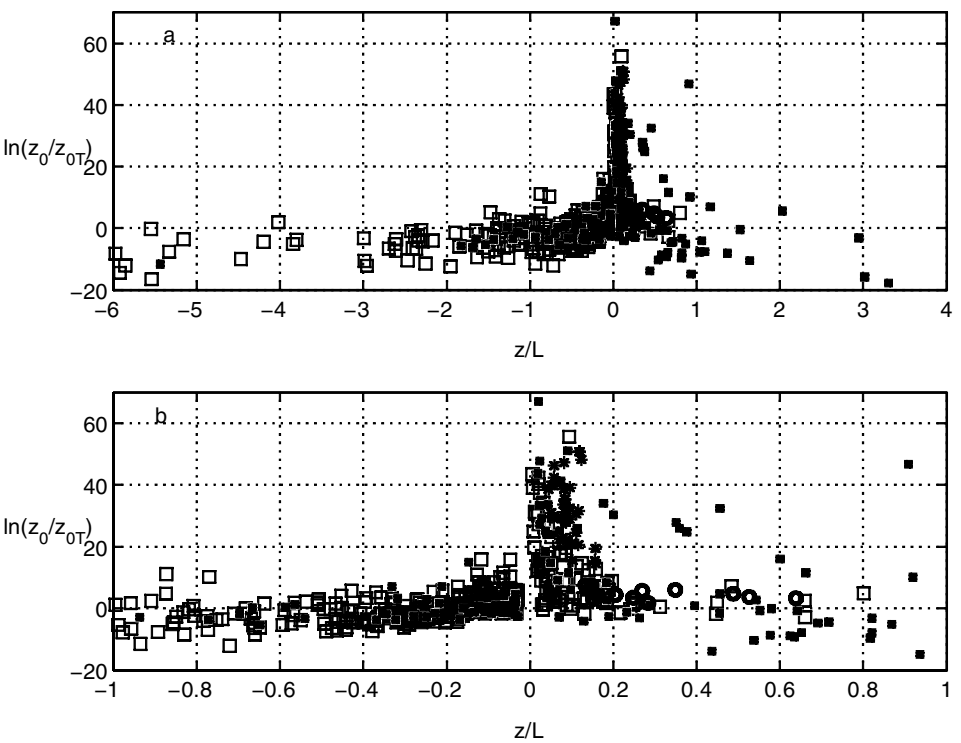

Figure 9. Function $\ln(z_0/z_{0T})$ plotted as a function of stability parameter, z/L(see section 3) for two stability ranges. Symbols are as in Fig. 5. See text for discussion.

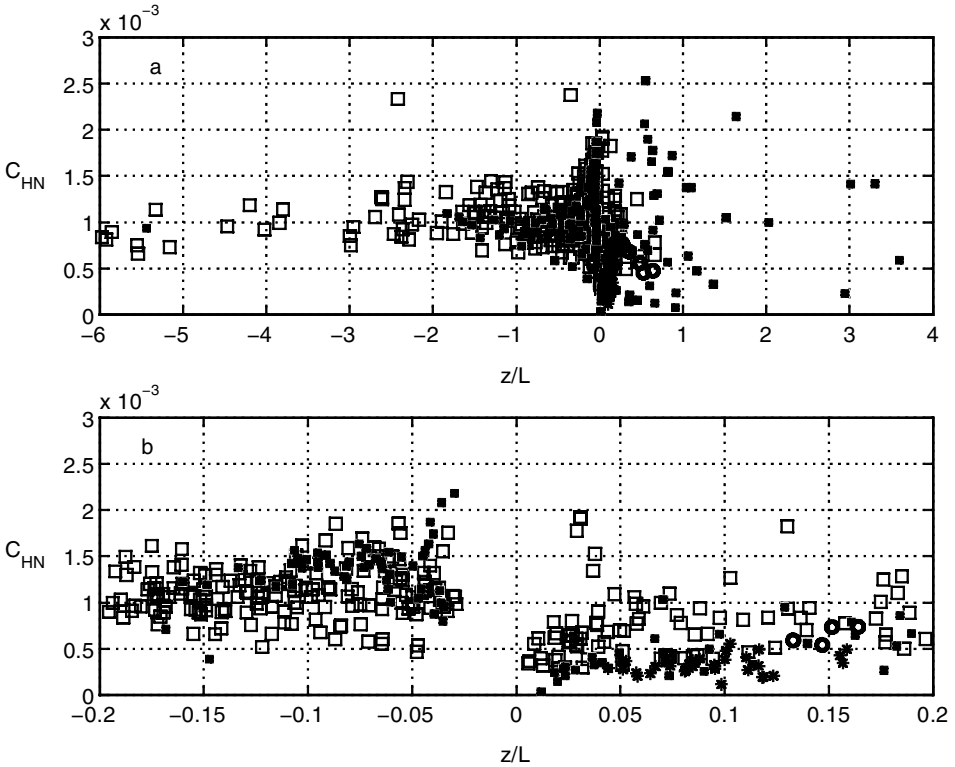

Figure 10. Neutral Stanton number, C_{HN}, plotted as a function of stability parameter z/L (see section 3) in: (a) the entire stability range $-6 < z/L < 4$, and (b) the near-neutral range, $-0.2 < z/L < 0.2$. Symbols are as in Fig. 5.

< 4, and for the near-neutral range $-0.2 < z/L < 0.2$, respectively. Note that these plots, which are based on apparent z_0 and z_{0T} values, must be regarded as plots of *apparent* C_{HN} values. This explains why the data display a pronounced variation with z/L, which would not have been expected if the reduction of C_H to neutrality through Eq. (13) had been accurate. Thus, the failure of the data in Figs. 10(a) and (b) to be independent of z/L must be considered as a strong indication that MO theory is inadequate to handle the sensible-heat exchange process in the MABL.

The plots of Figs. 10(a) and (b) bear strong similarity to the plot of C_H in Fig. 6. Most notable is the rapid drop of the data in the range $-0.05 < z/L < 0.0$ and the very low C_{HN} values on the stable side, particularly for the more reliable data obtained with the MIUU instrument.

In Fig. 11 C_{HN} has been plotted as a function of wind speed; Figs. 11(a) and (b) show data for $z/L < 0$ and for $z/L \geqslant 0$, respectively. Three curves have been drawn: those marked 'COARE' and 'Zeng' are based on the surface renewal schemes of Fairall *et al.* (1996a) and Zeng *et al.* (1998), respectively; the curve marked 'Oost' is a regression curve derived by Oost *et al.* (2000) from their field experimental data from the Meetpost Nordwijk in the North Sea. It is noteworthy that the two 'theoretical' estimates describe our unstable data well up to about 10 m s^{-1}. With increasing wind speed our data deviate upward compared with these curves, to an extent that increases rapidly with wind speed.

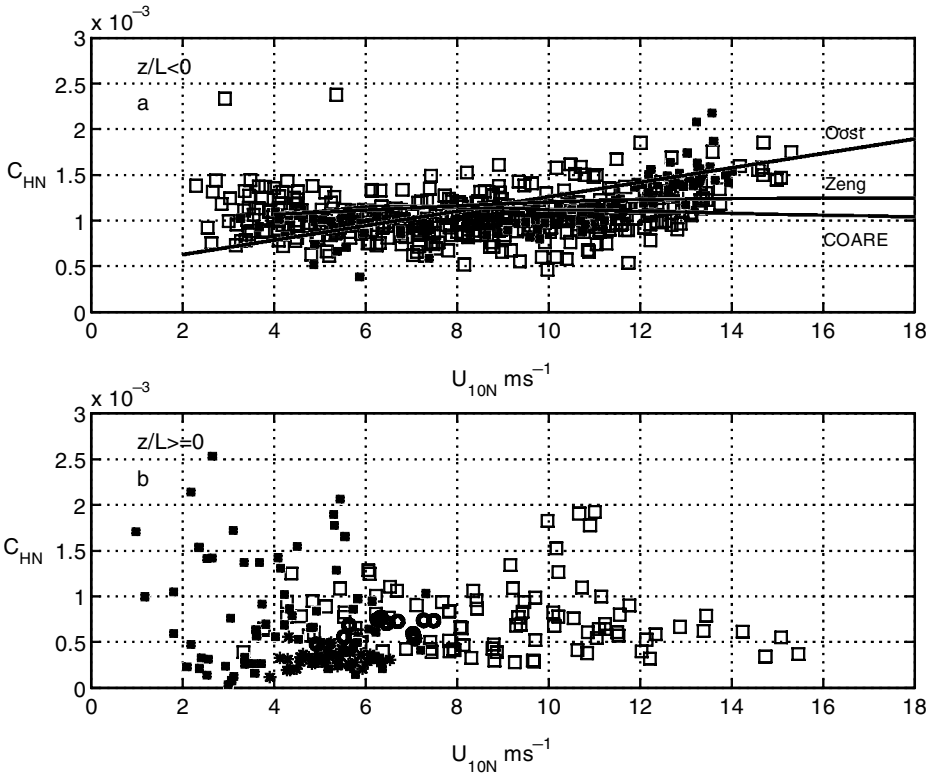

Figure 11. Neutral Stanton number, C_{HN}, plotted as a function of wind speed at 10 m for: (a) stability parameter $z/L < 0$, and (b) $z/L \geqslant 0$. The curves represent expressions from Oost *et al.* (2000), Fairall *et al.* (1996a; labelled COARE) and Zeng *et al.* (1998). Symbols are as in Fig. 5. See text for further details.

5. Discussion

Many marine field experiments have found that C_{HN} appears to be constant during unstable conditions, having a value around 1.1×10^{-3} (e.g. Smith 1980; Large and Pond 1982; DeCosmo *et al.* 1996). Most field studies also agree that C_{HN} is lower during stable conditions, with constant (but lower) values for this range as well. On the other hand, as mentioned in subsection 3(b), studies based on surface-renewal theory and laboratory data (e.g. Clayson *et al.* 1996; Fairall *et al.* 1996a; Zeng *et al.* 1998) give predictions which imply that C_{HN} should decrease at high wind speeds. All three tested these predictions on data from the tropical ocean and claim good agreement with theory. There are, however, no data with wind speed above 10 m s^{-1} in these studies.

Andreas and DeCosmo (2002) in their reanalysis of the HEXOS data (cf. subsection 3(b)) find that for conditions with high wind speeds the spray contribution is 'about 10% of the total flux' and '20–30% of the flux in ten of the 14 runs with strongest winds and have significant wave heights that are among the highest in our dataset'.

Going back to Fig. 11(a) of the present study, it is a reasonable interpretation that the observed deviation of our data at high wind speeds from the prediction of the two 'surface-renewal' models (the Zeng *et al.* (1998) and COARE models) is due to the effect of spray on the sensible-heat flux. Table 1 quantifies the deviation for the unstable cases. The last two columns give the ratio between the measured mean

TABLE 1. COMPARISON OF NEUTRAL C_{HN} VALUES FOR UNSTABLE CONDITIONS

U_{10}	$(C_{HN})_m \times 10^3$	$(C_{HN})_Z \times 10^3$	$(C_{HN})_F \times 10^3$	$(C_{HN})_m/(C_{HN})_Z$	$(C_{HN})_m/(C_{HN})_F$
10	1.0	1.20	1.12	0.83	0.89
12	1.2	1.23	1.10	0.98	1.09
14	1.5	1.24	1.10	1.21	1.37

Column 1 is the wind speed at 10 m (m s^{-1}). C_{HN} (Stanton number) values with subscripts m, Z and F are taken from this study, Zeng *et al.* (1998) and Fairall *et al.* (1996), respectively.

and corresponding estimated value obtained with the Zeng and the COARE method, respectively. At 12 m s^{-1} the ratios are still near unity, increasing to 1.21 at 14 m s^{-1} for the Zeng and 1.37 for the COARE method.

Note that when the wind speed is in the range 14–15 m s^{-1} and stability goes from slightly unstable to slightly stable, C_{HN} changes dramatically from about 1.5×10^{-3} to 0.5×10^{-3}. This is an effect that can be easily understood in terms of the theory for the spray-mediated flux contribution. As shown in Andreas (1992) and Andreas and DeCosmo (2002), the contribution from spray evaporation to the sensible-heat flux is proportional to $(T_s - T_{ev})$, where T_{ev} is 'a quasi-equilibrium temperature that the droplet falls to before evaporation begins in earnest'. The factor of proportionality contains the spray generation function and is positive. Thus, we expect that when in high wind conditions the temperature gradient near the surface changes from very slightly unstable to very slightly stable, other factors remaining essentially unaltered, the spray-mediated contribution to the sensible-heat flux remains the same, i.e. it is expected to increase the upward directed flux in the unstable case and reduce the downward directed flux to virtually the same extent.

The observed relative increase in the flux of sensible heat due to spray in this study is higher than the corresponding increase reported by Andreas and DeCosmo (2002). A reviewer suggested that this increase might be due to 'significant shoaling and consequent spray generation at the site'. On-site observations by one of the authors (AS) in conditions with a 15 m s^{-1} wind refutes this supposition: only one wave was observed to break at the shore and local spray generation was limited. Thus it is fair to assume that the footprint argument discussed in subsection 2(a) is also valid in the case of a 15 m s^{-1} wind, and hence that the observed spray effect is due to wave-breaking well outside the possible shoaling zone. Andreas and DeCosmo (2002) make the observation that the spray effect is closely linked to the significant wave height, and they notice (their Fig. 3) that for a certain wind speed this quantity is much less at the HEXOS site compared to what would be expected over the deep ocean. This is due to the fact that water is only 18 m deep at that site. As noted in subsection 2(a), the water depth at Östergarnsholm increases with distance offshore, reaching more than 50 m at 10 km from the island. Thus there is a possibility that a larger significant wave height is obtained at Östergarnsholm, causing a stronger spray effect. In fact, a plot of significant wave height, H_s, as a function of U_{10} at Östergarnsholm (not shown here) shows that H_s is 4.0 m at 15 m s^{-1}, which should be compared with the value of about 2.5 m obtained for the same wind speed in the HEXOS experiment.

The observed dramatic decrease in z_{0T} for near-neutral stable conditions (Fig. 6) can be understood as a result of the above findings. Equation (13) can be re-arranged:

$$\ln z_{0T} = \ln z - \frac{\kappa^2}{C_{HN} \cdot \ln(z/z_0)}.$$

From Fig. 8 it is clear that z_0 does not change very much from slightly unstable to slightly stable conditions. This means that the change in z_{0T} in this range is entirely due to the change in C_{HN}. With $z_0 = 10^{-4}$ m, taking $C_{HN} = 1.5\times10^{-3}$ for slightly unstable and 0.5×10^{-3} for slightly stable conditions, $z = 10$ m, and $\kappa = 0.4$, the above equation gives: $z_{0T} = 10^{-3}$ m for unstable and 10^{-11} m for stable conditions.

As seen from Fig. 11, the general level of C_{HN} for stable conditions is significantly lower than for unstable conditions. For $U_{10} > 12$ m s^{-1}, $C_{HN} \approx 0.5\times10^{-3}$ as noted above. For $U_{10} < 12$ m s^{-1}, the mean value is higher, circa 0.75×10^{-3}, in general agreement with previous findings (e.g. Smith 1980; Large and Pond 1982; Oost *et al.* 2000). The low values of C_{HN} for $U_{10} < 6$ m s^{-1}, where we do not expect spray effects, are intriguing. In Fig. 7(b), where z_{0T} is plotted against U_{10}, the prediction from surface renewal theory by Liu *et al.* (1979) is also included. This curve appears to represent more or less the upper bound for the very scattered data. No doubt, there are several possible factors that may influence the value of C_{HN} and z_{0T} in stable conditions. One such factor is discussed below: the effect of a low-level wind maximum, cf. subsection 3(e).

In Figs. 7(b) and 11(b), the stars represent cases from Nässkär when a wind maximum was observed in the height range 40–300 m above the water surface; the open circles represent cases from the same site without such a low-level wind maximum present. Note that the data representing cases with no low-level jet, cluster not far below the Liu *et al.* (1979) curve, whereas the stars fall much below the curve. The interpretation is made that this is due to the shear-sheltering effect (subsection 3(e) and Smedman *et al.* (2004)). The filled squares in Figs. 7(b) and 11(b) represent cases from an experiment at Östergarnsholm in the spring of 1995, when low-level jets were also often, but not always, present. Unfortunately, the pilot-balloon wind soundings were too few during this experiment to make a clear subdivision possible between occasions with and without a low-level wind maximum. Smedman *et al.* (1997) discussed the strong suppression of both the momentum exchange and the exchange of sensible heat during parts of their experiment. There are many open squares below the curve in Fig. 7(b) in the wind speed range 7–12 m s^{-1}. These data were obtained with an unattended sonic anemometer, and nothing is known about the possible presence of a low-level wind maximum in these particular cases. However, there are no reasons to exclude the possibility that there were in fact low-level jets present—climatologically these phenomena seem to be very common over the Baltic Sea in situations with warm air flowing over colder water. The cases allegedly influenced by shear sheltering (the stars) have a mean C_{HN} value of only 0.3×10^{-3}, i.e. less than half the typical stable value.

6. Conclusions

- The present study has shown that surface-renewal theory gives predictions for the exchange of sensible-heat flux over the sea that are in good agreement with measurements for *unstable* conditions and *wind speed less than about* 10 m s^{-1}.
- For higher wind speeds, spray-mediated effects increase the effective flux, so that at 14 m s^{-1} this effect amounts to as much as 20–40%. This result strongly corroborates the re-analysis of the HEXOS data by Andreas and DeCosmo (2002).
- As stability changes from very slightly unstable to very slightly stable in high wind speed conditions (around 15 m s^{-1}), a dramatic drop in C_{HN} occurs from about 1.5×10^{-3} to 0.5×10^{-3}. This is in qualitative agreement with the idea of a spray-mediated increase of the sensible-heat flux, which does not necessarily change sign when the temperature gradient in the surface layer changes sign.

• For stable conditions large scatter is found in the C_{HN} estimates. In general agreement with many previous studies, values are found to be about 30% lower in the mean than for corresponding unstable conditions.

• Analysis of certain datasets during stable conditions for which wind profiles throughout the boundary layer are available, indicates that the presence of a low-level wind maximum appears to strongly suppress the surface heat flux, in agreement with predictions about shear sheltering. In corresponding cases without such a low-level wind maximum present, the C_{HN} values come close to the curve derived from surface-renewal theory.

Acknowledgements

This work was funded by the Swedish Natural Science Research Council (NFR contract G5103-1340/1999). We wish to thank Dr Hans Bergström for supplying the Nässkär data and for performing the measurements together with other members of the MIUU staff. We also thank Dr Kimmo Kahma and Ms Heidi Pettersson from the Finnish Institute of Marine Research, Helsinki, Finland for providing the wave buoy data.

References

Andreas, E. 1992 Sea spray and the turbulent air–sea heat fluxes. *J. Geophys. Res.*, **97,** 11429–11441

Andreas, E. and DeCosmo, J. 2002 The signature of sea spray in the HEXOS turbulent heat flux data. *Boundary-Layer Meteorol.*, **103**, 303–333

Bergström, H. and Högström, U. 1987 Calibration of a three-axial fiber-film system for meteorological turbulence measurements. *Dantec Information*, **5,** 16–20

Bergström, H. and Smedman, A. 1995 Stably stratified flow in a marine atmospheric surface layer. *Boundary-Layer Meteorol.*, **72,** 239–265

Clayson, C. A., Fairall, C. W. and Curry, J. A. 1996 Evaluation of turbulent fluxes at the ocean surface using surface renewal theory. *J. Geophys. Res.*, **101,** 28503–28513

DeCosmo, J., Katsaros, K. B., Smith, S. D., Anderson, R. J., Oost, W. A., Bumke, K. and Chadwick, H. 1996 Air–sea exchange of water vapor and sensible heat: The Humidity Exchange Over the Sea (HEXOS) results. *J. Geophys. Res.*, **101,** 12001–12016

Drennan, W. M., Graber, H. C., Hauser, D. and Quentin, C. 2003 On the wave age dependence of wind stress over pure wind seas. *J. Geophys. Res.*, **108**(C3), 8062, doi: 10.1029/2000JC000715

Fairall, C. W., Bradley, E. F., Rogers, D. P., Edson, J. P. and Young, G. S. 1996a Bulk parameterization of air–sea fluxes for the Tropical Ocean–Global Atmosphere Coupled-Ocean Atmospheric Response Experiment. *J. Geophys. Res.*, **101,** 3747–3764

Fairall, C. W., Bradley, E. F., Godfrey, J. S., Wick, G. A., Edson, J. P. and Young, G. S. 1996b Cool-skin and warm-layer effects on the sea surface temperature. *J. Geophys. Res.*, **101,** 1295–1308

Grelle, A. and Lindroth, A. 1994 Flow distortion by a Solent sonic anemometer: Wind tunnel calibration and its assessment for flux measurements over forest and field. *J. Atmos. Oceanic. Technol.*, **11,** 1529–1542

Högström, U. 1988 Non-dimensional wind and temperature profiles in the atmospheric surface layer. *Boundary-Layer Meteorol.*, **42,** 263–270

1996 Review of some basic characteristics of the atmospheric surface layer. *Boundary-Layer Meteorol.*, **78,** 215–246

2001 'Results of turbulence instrument inter-comparison in the field'. MIUU Autoflux Report. Department of Earth Sciences, Meteorology Institute Uppsala University, Sweden (also: www.soc.soton.ac.uk/JRD/MET/AUTOFLUX/)

Högström, U. and Smedman, A. 2004 Accuracy of sonic anemometers: Laminar wind tunnel calibrations compared to atmospheric *in situ* calibration against a reference instrument. *Boundary-Layer Meteorol.*, **111**(1), 33–54

Hunt, J. C. R. and Durbin, P. A. 1999 Perturbed vortical layers and shear sheltering. *Fluid Dyn. Res.*, **24,** 375–404

Johansson, C. 2003 'Influence of external factors on the turbulence structure in the atmospheric boundary layer'. Acta Universitatis Upsaliensis. Comprehensive summaries of Uppsala dissertations from the Faculty of Science and Technology 792. Uppsala University, Sweden

Johansson, C., Smedman, A., Högström, U., Brasseur, J. G. and Khanna, S. 2001 Critical test of the validity of Monin–Obukhov similarity during convective conditions. *J. Atmos. Sci.*, **58,** 1549–1566

Kaimal, J. C. and Gaynor, J. E. 1991 Another look at sonic anemometry. *Boundary-Layer Meteorol.*, **56,** 401–410

Large, W. G. and Pond, S. 1982 Sensible and latent heat flux measurements over the ocean. *J. Phys. Oceanogr.*, **12,** 464–482

Liu, W. T., Katsaros, K. B. and Businger, J. A. 1979 Bulk parameterization of air–sea exchanges of heat and water vapor including the molecular constraints at the interface. *J. Atmos. Sci.*, **36,** 1722–1735

Lumley, J. L. and Panofsky, H. A. 1964 *The structure of atmospheric turbulence*. Interscience Publishers, New York, USA

Oost, W. A., Jacobs, C. M. and van Oort, C. 2000 Stability effects on heat and moisture fluxes at sea. *Boundary-Layer Meteorol.*, **95,** 271–302

Rutgersson, A., Smedman, A. and Omstedt, A. 2001 Measured and simulated sensible and latent heat fluxes at two marine sites in the Baltic Sea. *Boundary-Layer Meteorol.*, **99,** 53–84

Smedman, A. and Högström, U. 1973 The Marsta micro-meteorological field project: Profile measurement system and some preliminary data. *Boundary-Layer Meteorol.*, **5,** 259–273

Smedman, A. and Lundin, K. 1986 Influence of sensor configuration on measurements of dry and wet bulb temperature fluctuations. *J. Atmos. Oceanic Technol.*, **4,** 668–673

Smedman, A., Lundin, K., Bergström, H. and Högström, U. 1991 A precision kite or balloon borne mini-sonde system for wind and turbulence measurements. *Boundary-Layer Meteorol.*, **56,** 295–307

Smedman, A., Bergström, H. and Högström, U. 1995 Spectra, variances and length scales in a marine stable boundary layer dominated by a low level jet. *Boundary-Layer Meteorol.*, **76,** 211–232

Smedman, A., Högström, U. and Bergström, H. 1997 The turbulence regime of a very stable marine airflow with quasi-frictional decoupling. *J. Geophys. Res.*, **102,** 21049–21059

Smedman, A., Högström, U., Bergström, H., Rutgersson, A., Kahma, K. K. and Pettersson, H. 1999 A case study of air–sea interaction during swell conditions. *J. Geophys. Res.*, **104,** 25833–25851

Smedman, A., Guo Larsén, X., Högström, U., Kahma, K. K. and Pettersson, H. 2003 The effect of sea state on the momentum exchange over the sea during neutral conditions. *J. Geophys. Res.*, **108**(C11), 3367, doi: 10.1029/2002.JC001526

Smedman, A., Högström, U. and Hunt, J. C. R. 2004 Effects of shear sheltering in a stable atmospheric boundary layer with strong shear. *Q. J. R. Meteorol. Soc.*, **126,** 31–50

Smith, S. D. 1980 Wind stress and heat flux over the ocean in gale force winds. *J. Phys. Oceanogr.*, **10,** 709–726

Zeng, X., Zao, M. and Dickinson, R. E. 1998 Intercomparison of bulk aerodynamic algorithms for the computation of sea surface fluxes using TOGA COARE and TAO data. *J. Climate*, **11,** 2628–2644